

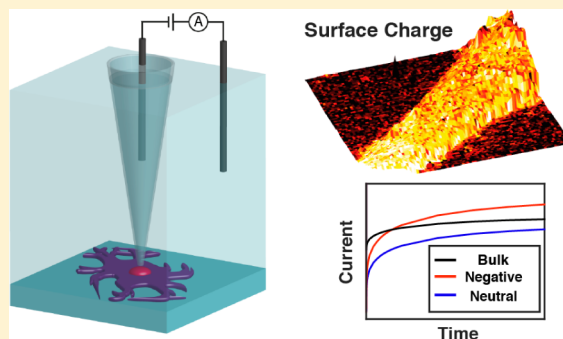
Fast Nanoscale Surface Charge Mapping with Pulsed-Potential Scanning Ion Conductance Microscopy

Ashley Page,^{†,‡,¶} David Perry,^{†,‡,¶} Philip Young,[§] Daniel Mitchell,^{||} Bruno G. Frenguelli,[§] and Patrick R. Unwin^{*,†}

[†]Department of Chemistry, [‡]MOAC Doctoral Training Centre, [§]School of Life Sciences, and ^{||}Warwick Medical School, University of Warwick, Coventry, CV4 7AL, United Kingdom

S Supporting Information

ABSTRACT: A vast range of interfacial systems exhibit charge heterogeneities on the nanoscale. These differences in local surface charge density are challenging to visualize, but recent work has shown the scanning ion conductance microscope (SICM) to be a very promising tool to spatially resolve and map surface charge and topography via a hopping potential sweep technique with a single nanopipette probe, with harmonic modulation of a bias applied between quasi-reference counter electrodes in the nanopipette and bulk solution, coupled with lock-in detection. Although powerful, this is a relatively slow process, with limitations on resolution and the size of the images that can be collected. Herein, we demonstrate a new scanning routine for mapping surface charge and topography with SICM, which increases the data acquisition rate by an order of magnitude and with the potential for further gains. Furthermore, the method is simplified, eliminating the need for bias modulation lock-in detection, by utilizing a potential-pulse, chronoamperometric approach, with self-referencing calibration of the response at each pixel in the image. We demonstrate the application of this new method to both a model substrate and living PC-12 cells under physiological (high ionic strength) conditions, where charge mapping is most challenging (small Debye length). This work contributes significantly to the emergence of SICM as a multifunctional technique for simultaneously probing interfacial structure and function with nanometer resolution.



Scanning ion conductance microscopy (SICM) is a powerful technique for nanoscale noncontact imaging of surface topography^{1–3} that finds particular application in the study of cellular systems,^{4–8} where resolution has been extended to the individual protein level⁹ and is comparable to atomic force microscopy (AFM).¹⁰ SICM utilizes a nanopipette filled with electrolyte to probe an interface that is also bathed in electrolyte. A bias is applied between a quasi-reference counter electrode (QRCE) in the nanopipette and one in bulk solution to generate an ionic current. Changes in the ionic current as the nanopipette approaches the substrate can be used to sense and provide information about the interface.

Recent developments have taken SICM beyond topography and shown that the current response may be inherently sensitive to other interfacial properties, most notably surface charge heterogeneities^{11–13} and surface reactions.¹⁴ Local changes in ionic conductivity near an interface affect the SICM current and can thus be mapped and analyzed, for example, with finite element method (FEM) modeling.^{15–17} All of these applications require careful consideration of the scanning routine used, particularly the applied potential bias, so that SICM provides unambiguous information on surface properties.

However, it has been shown that, without careful experimental design, the topographical and surface charge data obtained with SICM can become convoluted, affecting the accuracy of these studies. To address this issue, surface charge mapping with SICM has been performed in a bias modulated (BM)-SICM¹⁸ format that enables topography and surface charge to be resolved simultaneously without convolution.¹² In this regime, the nanopipette is approached to the surface or interface of interest, with no net (time-averaged) bias applied between the two QRCEs, just a small harmonic oscillation of the bias around 0 V. Importantly, this renders the SICM response relatively insensitive to surface charge, so that topography is mapped faithfully. Upon detection of the substrate (usually by a change of the current phase), the bias is then swept between two extreme values and the SICM response becomes sensitive to surface charge. The surface charge is elucidated by comparing the voltammogram near the surface to one performed in bulk at each and every pixel in a self-referencing regime.

Received: September 22, 2016

Accepted: October 24, 2016

Published: October 24, 2016

In this contribution, we introduce a new regime that significantly advances SICM topography-charge mapping, increasing the pixel acquisition rate by an order of magnitude (with scope for further gains), thereby allowing for imaging with a much higher pixel density. The method eliminates the modulation of the bias and replaces this with a minimal fixed bias that permits faster approach speeds for topographical imaging, while a pulse in the bias at the point of closest approach, as opposed to a voltammogram, and allows faster acquisition of surface charge information. Voltage-switching has proved useful in the related technique of scanning electrochemical microscopy (SECM), for topography and activity imaging with a single solid nanoelectrode probe, but requires the use of two redox mediators in solution which may be somewhat restrictive.¹⁹ FEM simulations allow for the quantification of the experimental data and show no loss of accuracy when compared to the previous potential-scanning regime.¹² The increase in pixel density afforded by this new approach reveals previously unseen charge heterogeneities in two substrates: an interrupted polystyrene film in high electrolyte concentration and a neuron-like PC-12 cell imaged in cell culture media. Thus, the reliable increase of the scanning speed improves the viability of SICM as a multifunctional technique for surface charge mapping on the nanoscale and offers new control functions that could be applied to other SICM methods.

MATERIALS AND METHODS

Solutions. Milli-Q reagent grade water (resistivity ca. 18.2 M Ω cm at 25 °C) was used for all solutions. 50 mM KCl (Sigma-Aldrich) was used for the SICM charge maps of the interrupted polystyrene film on glass. PC-12 cells were cultured and imaged in RPMI 1640 media containing 15% horse serum, 2.5% fetal calf serum, 5 mM glutamine, 100 U/mL penicillin, and 100 μ g/mL streptomycin (all Sigma-Aldrich).

Nanopipettes and Electrodes. Nanopipettes were pulled from borosilicate glass capillaries (o.d. 1.2 mm, i.d. 0.69 mm, Harvard Apparatus) using a laser puller (P-2000, Sutter Instruments; pulling parameters: Line 1: Heat 330, Fil 3, Vel 30, Del 220, Pul -; Line 2: Heat 330, Fil 3, Vel 40, Del 180, Pul 120). The inner radius of the probe was measured using a JEOL 2000FX transmission electron microscope (TEM) to be 80 ± 15 nm (see Table S1 for experimental geometries of the two probes used). Two Ag/AgCl electrodes were used, one in the nanopipette and a second in bulk solution.

Substrates. Glass-bottomed Petri dishes with detachable coverslips (3512, WillcoWells) were used for both substrates. In the case of the polystyrene, the glass bottom of the dish was dip-coated in a solution of polystyrene dissolved in chloroform (1 mg/mL) to ensure a heterogeneous substrate. The PC-12 cells used were adherent to glass-bottomed Petri dishes, and so, these were used as a support.

Cell Culturing Procedure. Adherent PC-12 cells (ATCC-CRL-1721.1) were cultured in tissue culture flasks in the above-specified media until confluent, before trypsinization and transfer to Petri dishes. They were allowed 72 h to adhere to the glass substrate before imaging in fresh media.

Instrumentation. The basic instrumentation setup has been described in detail previously.^{12,20} Briefly, the lateral movement of the probe was controlled using a two-axis piezoelectric positioning system with a range of 300 μ m (Nano-BioS300, Mad City Laboratories, Inc.), while movement normal to the substrate was controlled using a more precise

piezoelectric positioning stage of range 38 μ m (P-753-3CD, Physik Instrumente). The electrometer and current–voltage converter used were both made in-house, while user control of probe position, voltage output, and data collection was via custom-made programs in LabVIEW (2013, National Instruments) through an FPGA card (7852R, National Instruments).

Fast Charge Mapping SICM. All images presented herein were collected using a self-referencing scan hopping mode of SICM, with the regime for each pixel as follows (Figure 1a): (I)

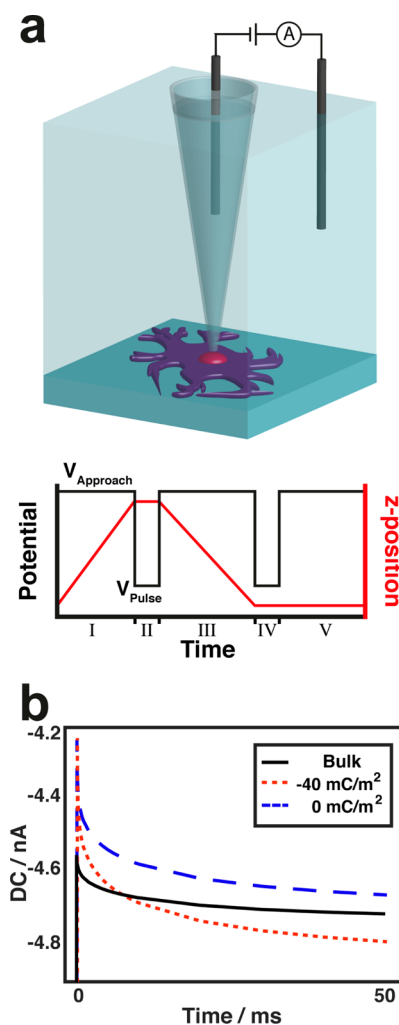


Figure 1. Setup for a high-speed charge mapping experiment. (a) Schematic of basic SICM setup used for charge mapping, with a trace of z -position and potential at each hop in the scan hopping regime: (I) probe approaches the surface at $V_{\text{Approach}} = +20$ mV, (II) 50 ms pulse at $V_{\text{Pulse}} = -400$ mV before (III) probe is retracted at +20 mV and (IV) a second pulse to -400 mV in bulk solution. (V) Probe is moved in the x or y direction to the next point. (b) Simulated I – t curves of a probe in bulk (black line) and at a 15 nm separation from surfaces of neutral and negative charge (red and blue lines, respectively).

First, the probe was translated toward the surface at 6 μ m/s with the QRCE in the probe biased at +20 mV vs the QRCE in bulk. When the ionic current between the two electrodes had reduced by a chosen threshold value (giving a precise working distance, as calculated from FEM simulations, see below), the probe motion was halted before (II) a 50 ms pulse of the probe potential to -400 mV. After this pulse (III), the probe potential was returned to +20 mV and the probe was retracted either 1 or

2 μm for the polystyrene or PC12 cell samples, respectively (retract distance dependent on the height variation of the substrate, but sufficient to represent bulk solution as it was always well over 5 times the dimensions of the nanopipette opening)¹ at 10 $\mu\text{m/s}$ before (IV) a second 50 ms pulse in the bulk solution; (V) the probe was then moved to the next pixel. The current was monitored during the entire process at a rate of 2 kHz, and the current–time (I – t) curve at the surface and the I – t curve in bulk were compared to extract surface charge information at each pixel.

FEM Simulations. A 2D axisymmetric model of the nanopipette in bulk solution and near a substrate was constructed in COMSOL Multiphysics (v. 5.2) with the Transport of Diluted Species and Electrostatics modules. A schematic of the simulation domain and boundary conditions is presented in Figure S2. The dimensions of the nanopipettes were extracted from TEM images of nanopipettes.^{21,22}

To obtain working distances for experimental SICM measurements, simulations were performed at varying probe–substrate separation with an applied probe bias of +20 mV (the experimental approach bias). Once the working distance, corresponding to the experimental feedback threshold was known, time-dependent simulations were performed at this separation distance with varying surface charge applied to the domain boundary below the nanopipette. Simulations were also performed with the nanopipette positioned in bulk solution and the near-surface values of the ionic current, with different applied surface charge, were normalized to those in bulk to elucidate surface charge from experimental maps. For all of these simulations, the initial conditions used were obtained from steady-state simulations performed with the same conditions except the tip bias was +20 mV (the approach bias).

■ RESULTS AND DISCUSSION

Scanning Regime for Interfacial Charge Mapping.

Previous work on SICM showed that the charge at an interface, particularly in low ionic strength electrolyte concentrations (≤ 10 mM aqueous solution), can have a significant effect on the current response during the approach of the nanopipette probe toward a substrate surface.^{11,12,23–25} This convolution of charge and topography becomes more significant as the potential difference between the two QRCEs is increased.¹² To overcome this problem, our previous work utilized a BM-SICM regime, which allowed topographical information to be extracted with no net bias and just a small harmonic perturbation, followed by the application of a linear scan of potential at each pixel to reveal the charge. However, the use of modulation-based SICM constrains the approach speed of the probe, depending on the time constant of the lock-in amplifier used and modulation frequency employed.¹⁸ Herein, we make use of a direct current (DC) feedback mode to generate a feedback signal for essentially *charge-insensitive topographical mapping*. In this setup, a small bias (+20 mV at the probe electrode with respect to the QRCE in bulk solution) is applied to produce the ionic current for DC feedback (topographical mapping). It was possible to apply such a small bias, which generated a reasonable current magnitude, because the experiments were carried out in physiologically relevant media, which has high ionic strength and will be most relevant for future work, e.g., for cell imaging. The choice of approach bias in these measurements is important and requires a theoretical consideration. The bias chosen will depend on the ionic strength of the imaging media and the size of the

nanopipette, as well as the range of surface charges that are to be probed. The bias needs to be chosen such that it provides a robust feedback signal for tracking topography experimentally, but simulations (such as those reported herein) are also required to justify that, under the imaging conditions, the surface charge of the substrate does not influence the nanopipette response. Upon approach to within a probe diameter of the substrate of interest, a decrease of the ionic current between the two QRCEs occurs² which is attributed to the increased access resistance near the nanopipette opening. This approach comfortably allows the mapping of topography at approach speeds of 5 $\mu\text{m/s}$ and above (maximum not tested). The small applied bias, as discussed below, meant that there was little convolution of the topography and charge at the interface in relatively high electrolyte concentrations (≥ 50 mM), and the current response allowed for accurate topographical mapping (see below).

As mentioned above, the extraction of interfacial charge information in previous work utilized the measurement of a cyclic voltammogram (CV) both at the surface and in bulk solution, considering the rectification of the current–voltage behavior as a result of the diffuse double layer (DDL) at the tip and surface.^{12,23,25} Typically, the CV was obtained by sweeping the potential between -400 and $+400$ mV at a scan rate of 1 V/s, a total of 3.2 s of CV time per pixel (1.6 s at the surface and 1.6 s in bulk). Despite the wealth of information collected at each pixel in this regime (including potential-resolved current–space movies), surface charge was manifested in the current response mostly at large bias. In fact, in our previous work, the FEM simulations for the quantification of surface charge were only carried out at the extreme potentials of the CV, with an applied potential of -400 mV proving to be the most sensitive to variations in local interfacial charge.¹²

In this work, the time taken to collect interfacial charge information is significantly reduced by pulsing the probe bias from the approach potential (+20 mV) to -400 mV at the point of closest approach and, in bulk, in a self-referencing format (Figure 1a). To prove the potential pulse concept, current–time (I – t) transients were simulated in 50 mM KCl (Figure 1b). For the three simulated I – t curves shown, the initial conditions were obtained by first performing a steady-state simulation at the approach probe potential (+20 mV) before a subsequent time-dependent simulation with an applied bias of -400 mV, with different surface charges applied to the substrate. The simulations at 0 and -40 mC/m² used a probe–substrate separation of 15 nm, which corresponded to the feedback threshold used during experiments, as obtained below. It is clear that the I – t response near the surface is different compared to the bulk solution and that, when the probe is near the surface, the charge has a significant influence on the response, validating the use of this new imaging methodology. In these conditions, a negatively charged surface caused an enhancement of the current while a neutral surface caused a diminution, when compared to the bulk response as explained in previous work.^{12,25} Further simulations produced working curves of normalized current as a function of surface charge for each of the experimental conditions below. For the present work, 50 ms was taken as the length of the experimental potential pulse, with the final few points of the surface I – t curve normalized with respect to the final few points of the bulk I – t curve at each pixel to produce spatially resolved surface charge maps. The significant improvements to both the approach speed and interfacial charge collection time reduce

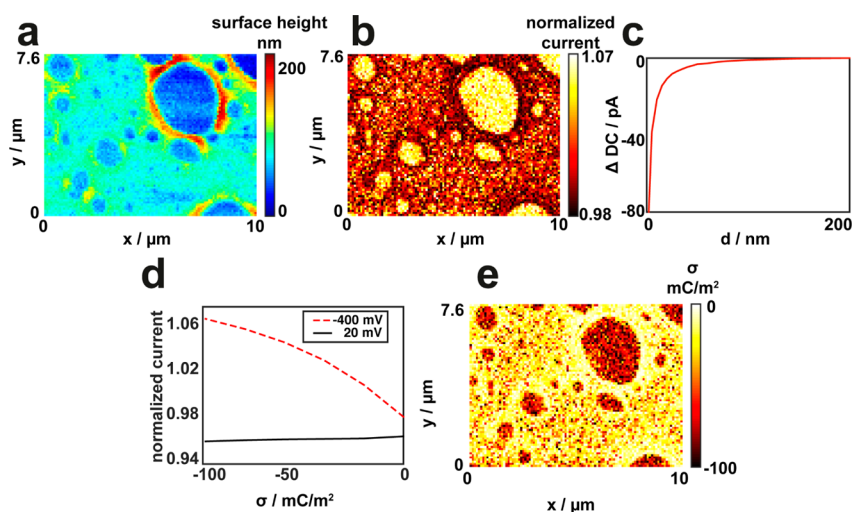


Figure 2. Simultaneous topography and quantified charge maps of an incomplete polystyrene film on a glass substrate. (a) Topography image recorded with a ~ 70 nm radius nanopipette in a hopping regime using DC feedback. (b) Normalized current (surface current divided by bulk current) map collected concurrently with the topography. (c) FEM simulation of the change in DC as the probe approaches the surface, showing dependence of probe–substrate separation on the feedback threshold chosen. (d) Simulated dependence of the normalized current on the charge at the surface, used to generate the quantified charge map in (e).

the typical pixel acquisition rate for this technique from over 5 s to less than 0.5 s, markedly increasing the efficacy and potential applications of SICM for localized surface charge mapping. Clearly, however, there would be scope for further improvement in the experimental time in the future, since differences in the I – t behavior are apparent on a few ms time scale (Figure 1b), and it should be possible to use piezoelectric positioners with a faster response than are used herein.

Validation of the Technique with a Polystyrene Film on Glass. The high-speed approach was first validated experimentally using an incomplete polystyrene film on a glass substrate, such that there were pinholes in the polystyrene layer, exposing the glass below to the solution. The topography from a typical scan, collected in 50 mM KCl with a DC feedback threshold (decrease in current from bulk to the point of closest approach) of 15 pA ($\sim 7\%$), is shown in Figure 2a, demonstrating a highly heterogeneous film that varies in thickness from a few tens of nm in some areas to a few hundreds of nm in others. Note that we applied an absolute change in the current, as the bulk current was found to be stable at 210 pA, but in situations where there was a change in the bulk current, a percentage change could easily be applied. Pinholes in the film in which the glass is exposed are of variable size, with some clearly visible and others not resolved as well, as they are the same size or smaller than the probe opening (~ 150 nm). The resolution of traditional SICM measurements and surface charge measurements is typically observed to be of a similar order of magnitude to the nanopipette dimensions ($0.5r$ – $1.5r$),¹ where r is the nanopipette opening radius and hence smaller nanopipettes would be required to resolve these features further.

The heterogeneities in the topography of the substrate are reproduced in the normalized current map (Figure 2b), obtained from the pulse procedure outlined above. Areas in which there is a large expanse of glass have normalized current values in the range of 1.05–1.07 (yellow/white coloring) while areas of thick polystyrene have normalized current values below 1 (dark red/black coloring). Interestingly, the intermediate areas of the scan largely have values between these two

extremes (red coloring), which can be attributed to pinholes on a scale less than that of the probe diameter. This explanation of the intermediary values of normalized current in those areas of the scan where the film is very thin also explain the wide range of values seen in these regions. If we denote the area of the substrate that affects the current response during the potential pulse as the “footprint” of the probe, then any value between the “true glass” value of ~ 1.06 and the “true polystyrene” value of ~ 0.99 could be obtained with differing percentages of glass and polystyrene in the footprint. A scan collected from a different sample in which the polystyrene is more uniform is presented in Figure S3 for comparison, which instead mainly shows just two regions of different charge.

An approach curve was simulated using the same probe geometry and electrolyte conditions as the experiment (Figure 2c) in order to extract the probe–substrate separation when a feedback threshold of 15 pA is used. From the approach curve, this value was found to be 15 nm, a separation that was then used for the time-dependent simulations at surfaces of differing charge density (Figure 2d). Note that further increases in the feedback threshold used could improve the sensitivity to charge heterogeneities. The red curve demonstrates a strong dependence of the normalized current on the surface charge density when the QRCE in the probe is biased at -400 mV, while at $+20$ mV (black curve) there is almost no effect of the surface charge on the normalized current, legitimizing the use of this potential during the approach for topographical imaging. The combination of the normalized current map in Figure 2b with the calibration curve in Figure 2d produced the quantified charge map in Figure 2e. Areas in which the polystyrene film is complete have a charge density of 0 mC/m², the expected value given the neutrality of the polymer, while glass has a charge of about -60 mC/m², comfortably within the range of those values quoted in the literature.²⁵ Note that the apparent surface charge in the glass regions is quite heterogeneous, most likely due to the heterogeneous distribution of the polymer film. For example, small patches of polystyrene are likely to be present within the predominantly glass regions. A typical scan collected using the bias modulation and CV approach in previous work is

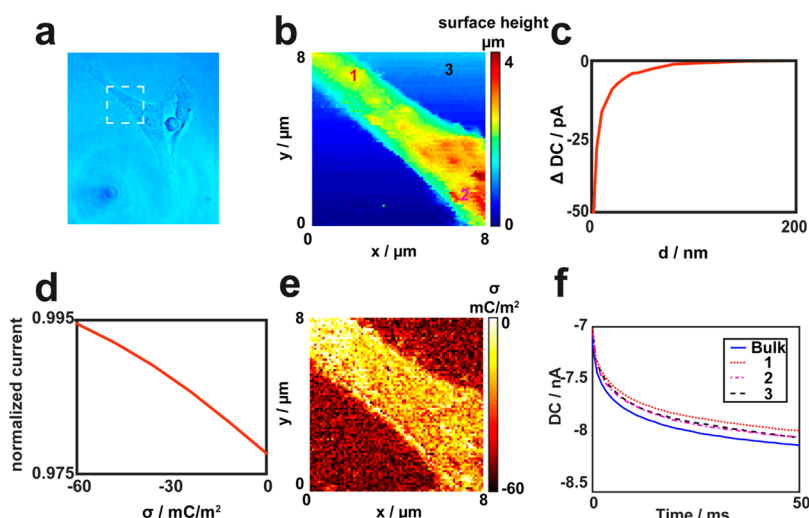


Figure 3. Simultaneous topography and charge maps of a PC-12 neurite on a glass substrate. (a) Optical image of the scanned cell, the white square showing the scan area. (b) Topographical image of the neurite, collected concurrently with the quantified charge map (e). (c) FEM simulation of the change in DC as the probe approaches the surface at +20 mV, showing dependence of probe–substrate separation on the feedback threshold chosen. (d) Simulated dependence of the normalized current on the charge at the surface, used to generate the quantified charge map in (e). Experimental I – t curves at the points of the scan labeled in (b) are shown in (f), along with a bulk I – t curve for comparison.

shown for comparison (Figure S4). The range of current values is larger as a lower electrolyte concentration (10 mM) was used, but the local charges are similar. It should be noted that despite containing significantly fewer pixels it took more than twice as long to obtain that image than the main scan presented in Figure 2.

Surface Charge Mapping of Neuron-like PC-12 Cells.

Having validated the use of high-speed charge mapping with SICM on a model substrate, we then investigated whether the technique could also be used in higher ionic strength conditions (~150 mM, RPMI 1640 media; see Materials and Methods for composition) in which the width of the DDL would be significantly reduced.²⁶ Figure 3a shows an optical micrograph of a spontaneously differentiated neuron-like cell from the PC-12 cell line, with the scan area, extending from the cell body along the length of a neurite, outlined by the dashed white square. The topographical data (Figure 3b), collected with a feedback threshold of 8 pA (~2%) and a working distance of 30 nm (see approach curve, Figure 3c), show that the region of the cell imaged varies in height by ~2 μm, with the thickest area at the cell body and the thinnest area toward the furthest extension of the neurite. Patches of increased height, several hundred nanometers in prominence, are seen along the length of the cell. The numbers on Figure 3b correspond to the experimental I – t curves in Figure 3f and highlight differences in charge between regions of the neurite (1), the cell body (2), and the glass (3). All three of these curves are lower in magnitude than a typical experimental bulk I – t curve (shown in blue). The compression of the range of possible normalized currents arises as a result of the decrease in double layer thickness, meaning the effect of charge density on ionic transport to the probe is diminished. Nonetheless, it is important to note that despite a range of only 1.5% in the normalized current across the entire scan (see Figure S5) the technique is still sensitive enough to quantify the charge density (Figures 3d,e).

As would be expected, the glass carries a homogeneous negative charge (~–50 to –60 mC/m²). While this value differs slightly from that obtained from the polystyrene scan

above, the two are not directly comparable. As the surface charge of glass relies on the acid–base equilibrium of silanol groups (SiOH) at the interface, the termination of which is dependent on the pH of the solution used. The 50 mM KCl had a pH of ~6.2 while the cell media was buffered to pH 7.2; a lower proportion of the silanol groups would be protonated in the media, and thus, a higher charge density would be expected. However, a lower surface charge is apparent in Figure 2. These small differences in the data for glass between Figures 2e and 3e are likely attributable to small polystyrene features within the glass region, which cannot be resolved topographically, which would serve to reduce the total surface charge presented in the nanopipette footprint. Additionally, the surface charge of the glass in the PC12 study could be impacted by the presence of other molecules (nutrients, proteins, etc.) in the cell growth (imaging) media, which could adsorb on the glass and alter its surface properties. In contrast to the glass substrate, the charge density of the PC-12 cell, though negative in polarity throughout, is highly heterogeneous. There is a gradient from the predominantly more negatively charged cell body (as highly charged as the glass in some areas; see Figure 3f, I – t curve 2) to the end of the less highly charged neurite (Figure 3f, I – t curve 1), though patches of lower charge also appear along the length of the cell. These heterogeneities could arise as a result of protein or charged-lipid rafts in the cell membrane, and further correlative techniques could probe the cellular function of these charge differences.

CONCLUSION

The image quality of interfacial charge mapping using SICM has been greatly improved by using a new tip approach and potential control function which increases the pixel acquisition rate by an order of magnitude, compared to our recently introduced format. The reduction in the time taken to acquire a single pixel of data was achieved via two separate improvements. First, approach speed of the probe was increased by changing the type of feedback used when detecting the surface. Second, the time taken to extract charge information in a given hop was reduced to 100 ms when previously it was in excess of

3 s. The resulting increase in image quality allowed the visualization of previously unseen features on the nanoscale, including ~100 nm defects in an interrupted polystyrene film and rafts of different charge at the surface of a neuron-like PC-12 cell. It should be noted that these studies present negative to neutral charges, but that the protocol would also be sensitive to positive surface charges, with enhanced sensitivity to such surface charges possible through tuning the pulse bias. It should be noted that these scans were collected using nanopipettes of ~80 nm radius, and with a decrease in size of the probes used, the resolution, and thus the power, of this technique could still be improved further. It should be possible to decrease the pulse time to a couple of ms and increase the approach speed with better piezoelectric positioners. This work contributes to the rise of SICM as a multifunctional technique, in this case allowing surface charge to be mapped with a resolution and image quality approaching that of the topographical mapping for which it is most commonly used.

■ ASSOCIATED CONTENT

■ Supporting Information

The Supporting Information is available free of charge on the ACS Publications website at DOI: [10.1021/acs.analchem.6b03744](https://doi.org/10.1021/acs.analchem.6b03744).

Dimensions of the probes used in the scans shown herein, along with a schematic of how those probes were modeled using FEM simulations; an additional scan over a polystyrene film and a calibration curve for the charge quantification over the PC-12 cell (PDF)

■ AUTHOR INFORMATION

Corresponding Author

*E-mail: p.r.unwin@warwick.ac.uk.

Author Contributions

†A.P. and D.P. contributed equally to this work.

Notes

The authors declare no competing financial interest.

■ ACKNOWLEDGMENTS

This work was supported by the EPSRC through the MOAC DTC, grant number EP/F500378/1. We thank Dr. Joanna Collingwood (School of Engineering, University of Warwick) for the use of her cell culturing facility and Minkyung Kang and Dr. Dmitry Momotenko for productive discourse about this work.

■ REFERENCES

- (1) Chen, C.-C.; Zhou, Y.; Baker, L. A. *Annu. Rev. Anal. Chem.* **2012**, *5*, 207–228.
- (2) Hansma, P. K.; Drake, B.; Marti, O.; Gould, S. A.; Prater, C. B. *Science* **1989**, *243*, 641–643.
- (3) Kranz, C. *Analyst* **2014**, *139*, 336–352.
- (4) Korchev, Y. E.; Bashford, C. L.; Milovanovic, M.; Vodyanoy, I.; Lab, M. J. *Biophys. J.* **1997**, *73*, 653–658.
- (5) Novak, P.; Li, C.; Shevchuk, A. I.; Stepanyan, R.; Caldwell, M.; Hughes, S.; Smart, T. G.; Gorelik, J.; Ostanin, V. P.; Lab, M. J.; Moss, G. W. J.; Frolenkov, G. I.; Klennerman, D.; Korchev, Y. E. *Nat. Methods* **2009**, *6*, 279–281.
- (6) Takahashi, Y.; Murakami, Y.; Nagamine, K.; Shiku, H.; Aoyagi, S.; Yasukawa, T.; Kanzaki, M.; Matsue, T. *Phys. Chem. Chem. Phys.* **2010**, *12*, 10012–10017.
- (7) Happel, P.; Thatenhorst, D.; Dietzel, I. D. *Sensors* **2012**, *12*, 14983–15008.
- (8) Nashimoto, Y.; Takahashi, Y.; Ida, H.; Matsumae, Y.; Ino, K.; Shiku, H.; Matsue, T. *Anal. Chem.* **2015**, *87*, 2542–2545.
- (9) Shevchuk, A. I.; Frolenkov, G. I.; Sanchez, D.; James, P. S.; Freedman, N.; Lab, M. J.; Jones, R.; Klennerman, D.; Korchev, Y. E. *Angew. Chem., Int. Ed.* **2006**, *45*, 2212–2216.
- (10) Rheinlaender, J.; Geisse, N. A.; Proksch, R.; Schäffer, T. E. *Langmuir* **2011**, *27*, 697–704.
- (11) McKelvey, K.; Kinnear, S. L.; Perry, D.; Momotenko, D.; Unwin, P. R. *J. Am. Chem. Soc.* **2014**, *136*, 13735–13744.
- (12) Perry, D.; Al Botros, R.; Momotenko, D.; Kinnear, S. L.; Unwin, P. R. *ACS Nano* **2015**, *9*, 7266–7276.
- (13) Perry, D.; Paulose Nadappuram, B.; Momotenko, D.; Voyias, P. D.; Page, A.; Tripathi, G.; Frenguelli, B. G.; Unwin, P. R. *J. Am. Chem. Soc.* **2016**, *138*, 3152–3160.
- (14) Momotenko, D.; McKelvey, K.; Kang, M.; Meloni, G. N.; Unwin, P. R. *Anal. Chem.* **2016**, *88*, 2838–2846.
- (15) Korchev, Y. E.; Negulyaev, Y. a; Edwards, C. R.; Vodyanoy, I.; Lab, M. J. *Nat. Cell Biol.* **2000**, *2*, 616–619.
- (16) Zhou, Y.; Chen, C. C.; Baker, L. A. *Anal. Chem.* **2012**, *84*, 3003–3009.
- (17) Novak, P.; Gorelik, J.; Vivekananda, U.; Shevchuk, A.; Ermolyuk, Y.; Bailey, R.; Bushby, A.; Moss, G. J.; Rusakov, D.; Klennerman, D.; Kullmann, D. M.; Volynski, K.; Korchev, Y. *Neuron* **2013**, *79*, 1067–1077.
- (18) McKelvey, K.; Perry, D.; Byers, J. C.; Colburn, A. W.; Unwin, P. R. *Anal. Chem.* **2014**, *86*, 3639–3646.
- (19) Takahashi, Y.; Shevchuk, A. I.; Novak, P.; Babakinejad, B.; Macpherson, J.; Unwin, P. R.; Shiku, H.; Gorelik, J.; Klennerman, D.; Korchev, Y. E.; Matsue, T. *Proc. Natl. Acad. Sci. U. S. A.* **2012**, *109*, 11540–11545.
- (20) McKelvey, K. M. Ph.D. Thesis, University of Warwick, 2012.
- (21) Perry, D.; Momotenko, D.; Lazenby, R. A.; Kang, M.; Unwin, P. R. *Anal. Chem.* **2016**, *88*, 5523–5530.
- (22) Sa, N.; Baker, L. J. *Electrochem. Soc.* **2013**, *160*, H376–H381.
- (23) Sa, N.; Baker, L. A. *J. Am. Chem. Soc.* **2011**, *133*, 10398–10401.
- (24) Clarke, R. W.; Zhukov, A.; Richards, O.; Johnson, N.; Ostanin, V.; Klennerman, D. *J. Am. Chem. Soc.* **2013**, *135*, 322–329.
- (25) Sa, N.; Lan, W. J.; Shi, W.; Baker, L. A. *ACS Nano* **2013**, *7* (12), 11272–11282.
- (26) Stumm, W.; Morgan, J. J. *Aquatic chemistry: chemical equilibria and rates in natural waters*, 3rd ed.; John Wiley & Sons: New York, 1996.